Available online at www.sciencedirect.com
ScienceDirect
Journal of Power Sources 160 (2006) 305–315
JOURNAL OF POWER SOURCES
www.elsevier.com/locate/jpowsour

Performance of intermediate temperature (600–800 °C) solid oxide fuel cell based on Sr and Mg doped lanthanum-gallate electrolyte

Wenquan Gong, Srikanth Gopalan, Uday B. Pal *

Department of Manufacturing Engineering, Boston University, MA 02215, United States

Received 10 November 2005; received in revised form 9 January 2006; accepted 11 January 2006
Available online 24 February 2006

Abstract

The solid electrolyte chosen for this investigation was $La_{0.9}Sr_{0.1}Ga_{0.8}Mg_{0.2}O_3$ (LSGM). To select appropriate electrode materials from a group of possible candidate materials, AC complex impedance spectroscopy studies were conducted between 600 and 800 °C on symmetrical cells that employed the LSGM electrolyte. Based on the results of the investigation, LSGM electrolyte supported solid oxide fuel cells (SOFCs) were fabricated with $La_{0.6}Sr_{0.4}Co_{0.8}Fe_{0.2}O_3$–$La_{0.9}Sr_{0.1}Ga_{0.8}Mg_{0.2}O_3$ (LSCF–LSGM) composite cathode and nickel–$Ce_{0.6}La_{0.4}O_2$ (Ni–LDC) composite anode having a barrier layer of $Ce_{0.6}La_{0.4}O_2$ (LDC) between the LSGM electrolyte and the Ni–LDC anode. Electrical performances of these cells were determined and the electrode polarization behavior as a function of cell current was modeled between 600 and 800 °C.

Keywords: Intermediate temperature solid oxide fuel cells; Materials system; Electrical performance

1. Introduction

The material property requirements for SOFCs are quite stringent and well established [1–4]. The electrolyte must have adequate oxygen-ion conductivity (>0.03 S cm^{-1}), negligible electronic conductivity, be stable in both oxidizing and reducing conditions and remain dense and impervious during cell operation. The porous and gas-permeable electrodes (anode and cathode) must have high electronic conductivity (>170 S cm^{-1}) and charge-transfer/surface exchange kinetics (>10^{-7} cm s^{-1}), be stable in respective gas environments (oxidizing conditions for cathode and reducing for anode) and remain chemically, mechanically and structurally compatible with the electrolyte and interconnect materials. The interconnect (bi-polar separator plate) material that connects the cathode of one cell to the anode of the next cell must be an electronic conductor, remain dense and impervious, be stable in both reducing and oxidizing conditions, and also be chemically, mechanically and structurally compatible with the anode and the cathode materials.

1.1. Limitations of the state-of-the-art SOFCs

Cathode-supported tubular SOFCs based on yttria-stabilized zirconia (YSZ) electrolyte, manufactured by Siemens Westinghouse are the most successful and robust cells to date and have shown power densities between 900 and 1100 °C up to 0.3 W cm^{-2} at a fuel utilization of 80–90% [5]. It has been recognized that the rather low power densities of these cells are attributed to the longer circumferential current path.

Planar single cells with a power density of 1.8 W cm^{-2} have been demonstrated using conventional YSZ thin film (∼5 μm) electrolytes supported on porous Ni–YSZ anodes at 800 °C. However, the power density decays to 0.8 W cm^{-2} at 700 °C [6]. The ultimate objective of the present work is to lower the operating temperature to 600–700 °C while maintaining a high power density. At high temperatures (≥800 °C) when operating the cells at current densities greater than 350 mA cm^{-2}, there are considerable interfacial reactions that occur at the electrode/electrolyte/interconnect interfaces. It causes cell degradation and densification of the porous cathode and thus limits the operating life of the cell. Lower operating temperatures will also allow the use of lower cost metallic interconnects and lower cost gas manifolding materials.

Tremendous progress has been made in extending the life of Simens Westinghouse SOFCs operating at 900–1100 °C, to

* Corresponding author. Tel.: +1 617 353 7708; fax: +1 617 353 5548.
E-mail address: upal@bu.edu (U.B. Pal).

0378-7753/$ – see front matter © 2006 Elsevier B.V. All rights reserved.
doi:10.1016/j.jpowsour.2006.01.039

more than 16,000 h with essentially less than 1% degradation in cell performance per 1000 h [7]. Since power densities of up to $\sim$2 W cm^{-2} have already been demonstrated using planar conventional YSZ-electrolyte-based cells at high temperatures, it is to be noted that if the operating temperature of the SOFCs is to be lowered, it is desirable that they also demonstrate comparable performance at lower temperature and have longer or comparable operating life. It is possible that a lower operating temperature can increase the operating life of the cells by reducing the interfacial reactions and decreasing the risk of delamination of the cell components during thermal cycling. However, a 300 °C decrease in the operating temperature from 1000 °C causes an order-of-magnitude increase of the zirconia electrolyte resistivity [2]. Therefore, if the operating temperature is lowered from 1000 to 700 °C, an order of magnitude thinner electrolyte (on the order of 2–5 μm) will be required to maintain similar ohmic loss. It is difficult to reliably deposit a continuous electrolyte of thickness on the order of 2–5 μm over electrodes having a comparable surface roughness, with a high yield, devoid of pin-holes and using low-cost manufacturing techniques. Also, the electrode kinetics has a strong exponential dependence on temperature and so employing the same electrodes at lower temperatures would result in significant polarization losses, particularly charge-transfer polarization losses at the electrode–electrolyte interfaces. This will drastically reduce the cell efficiency [3]. Hence, if the operating temperature of the SOFC is to be lowered below 800 °C, the electrode systems may also need to be changed.

1.2. Choice of electrolyte material for the intermediate temperature SOFC

Doped lanthanum gallate, $La_{0.9}Sr_{0.1}Ga_{0.8}Mg_{0.2}O_3$ (LSGM), was chosen as the electrolyte for lowering the operating temperature of the SOFC. The oxygen-ion conductivity of LSGM, doped ceria, doped bismuth oxide and doped zirconia are compared in Fig. 1 [8–10]. The primary advantage of selecting LSGM as the electrolyte material in this work is its stability

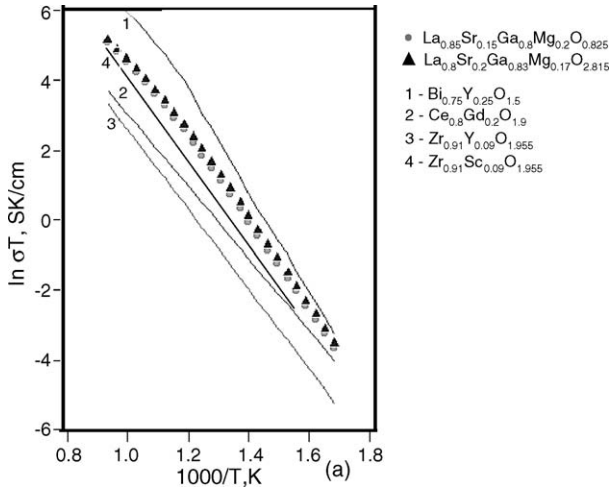

Fig. 1. Comparison of conductivities as a function of temperature of various oxygen-ion-conducting solid electrolytes [8].

and significantly higher oxygen-ion conductivity at lower temperatures compared to the other electrolytes (Fig. 1). Although scandia-doped zirconia also has high conductivity, its conductivity is known to decrease with time at temperature (aging effect) [10]. LSGM is very similar to YSZ in terms of its chemical stability. Kim and Yoo [11] have investigated LSGMs stability towards reduction in the P_{O_2} (oxygen partial pressure) range of 0.21–10^{-35} atm; conditions relevant to SOFC operation. They have reported that LSGM is stable and has an ionic transference number close to unity (>0.99) under these conditions. Based on superior oxygen-ion conductivity, negligible electronic conductivity and stability under SOFC operating conditions, LSGM is chosen as the electrolyte material for the intermediate temperature SOFC. However, issues such as material cost, Ga volatility, lower mechanical strength compared to the zirconia-based electrolyte, and manufacturability of electrode-supported SOFC will still need to be addressed.

1.3. Choice of electrode materials for the intermediate temperature SOFC

This work reports the performance in terms of the polarization resistance of several prospective anode and cathode materials for application in the intermediate temperature (600–800 °C) SOFCs employing LSGM electrolyte. The performance of a complete cell is described with the best performing cathode and anode materials systems. Cathode materials investigated included Sr-doped lanthanum manganite ($La_{1-x}Sr_xMnO_3$ or LSM), Sr and Fe doped lanthanum cobaltate ($La_{1-x}Sr_xCo_yFe_{1-y}O_3$ or LSCF), and two porous composite electrodes one comprising a two-phase particulate mixture of LSM–LSGM and the other consisting of LSCF–LSGM. These cathode materials have adequate electronic conductivity to function as a cathode [12] but their interfacial polarization resistance as a function of temperature needs to be determined because that is likely to influence their selection for application in the intermediate temperature SOFCs. The choice of anode materials focused on Ni-rare earth doped ceria composites. Nickel is a well-known SOFC anode material, and acts as the fuel side electrocatalyst and current collector. Usually the SOFC anodes are prepared by mixing and sintering NiO and an oxygen-ion-conducting oxide in air, followed by reducing the NiO to Ni under reducing conditions. Use of lanthanum or gadolinium doped ceria as the oxygen-ion-conducting oxide in the anode would buffer the thermal expansion mismatch between the anode and the electrolyte and also result in lowering the charge-transfer polarization due to its mixed-conducting property [13]; La- or Gd-doped ceria conducts both oxygen ions and electrons. It has been observed that the Ni phase in the anode reacts with the perovskite LSGM phase forming an insulating lanthanum nickelate phase and this also causes the ohmic and anodic polarization resistances to increase with time [14]. In response to this observation the concept of applying a thin (<5 μm) lanthanum or gadolinium doped ceria barrier layer to prevent direct contact and reaction of Ni with the LSGM electrolyte has been presented in this work. Since the doped ceria has sufficiently high oxygen-ion conductivity and the barrier layer is thin, it is not

expected to increase the ohmic polarization resistance of the cell.

1.4. Complete intermediate temperature solid oxide fuel cells

For the purpose of demonstration and ease of fabrication, LSGM electrolyte supported SOFCs with the most optimum cathode and anode materials system including the barrier layer between the electrolyte and the anode were electrochemically evaluated between 600 and 800 °C.

2. Experiments

2.1. Powder synthesis

Electrolyte powders of the composition $La_{0.9}Sr_{0.1}Ga_{0.8}Mg_{0.2}O_3$ (LSGM) were prepared by mixing and ball-milling precursors of lanthanum carbonate, strontium carbonate, gallium oxide and magnesium oxide in appropriate stoichiometric ratios and calcining at a temperature of 1200 °C for 4 h in air. The calcined powders were lightly crushed using alumina mortar and pestle and the calcination step was repeated for completing the solid-state reaction. Electrode materials such as $La_{0.9}Sr_{0.1}MnO_3$ (LSM), $La_{0.6}Sr_{0.4}Co_{0.8}Fe_{0.2}O_3$ (LSCF), $Ce_{0.85}Gd_{0.15}O_2$ (GDC) and $Ce_{0.6}La_{0.4}O_2$ (LDC) were also made using the same mixing and calcination techniques. X-ray powder diffraction analysis confirmed the composition, phase and purity of the material. All the synthesized powders (LSGM, LSM, LSCF, GDC, LDC) and NiO powder purchased from Baker were then separately ball-milled in methanol. Laser Scattering Particle Size Distribution Analyzer (Horiba LA-910) was periodically used at different intervals of the ball-milling process to determine the particle size and distribution. The ball-milling process was stopped when the desired particle size and distribution were obtained.

2.2. Conductivity measurement of LSGM electrolyte

For verification with literature measurements, the conductivity of the synthesized LSGM electrolyte was measured using a four-probe DC technique [15–17]. The measured conductivities are shown in Fig. 2. These measured conductivities are within 2–5% of the previously reported measurements [18–20].

2.3. Symmetrical cell fabrication

Calcined and milled LSGM powders at room temperature were die-pressed at 10,000 psi pressure into pellets and sintered in air at 1450 °C for 4 h. The sintered LSGM pellets were 1.4 mm thick and 2 cm in diameter. The LSGM pellets were then all finely ground to a uniform 1 mm thickness using diamond-grinding discs. LSM–LSGM, LSCF–LSGM, NiO–GDC, and NiO–LDC composite electrodes were prepared by thoroughly mixing desired amounts of the powders. The electrode powders (LSM, LSM–LSGM, LSCF, LSCF–LSGM, NiO–GDC, and NiO–LDC) were each dispersed in α-terpeniol solvent to form a paste. For the cathode electrodes (LSM, LSM–LSGM, LSCF, and LSCF–LSGM) and the anode without the barrier layer, the ground LSGM electrolyte pellets were masked with Scotch™ tape to form an outer ring on both sides and the electrode pastes were painted smoothly on the open circular surfaces. The painted LSGM electrolyte pellets were air-dried, masks removed and fired in air at elevated temperature for 2 h. The firing temperature was 1100 °C for all the cathodes and 1200–1300 °C for the anodes (i.e. NiO–GDC and Ni–LDC electrode samples). All electrodes had the same effective area of around 1.33 cm^2. When GDC or LDC barrier layers were employed between the Ni-doped-ceria composite anode and the LSGM electrolyte, very fine GDC or LDC powders were dispersed in α-terpeniol solvent to form a paste which was painted on both sides of the LSGM electrolyte. They were air-dried and sintered at 1200–1300 °C and the anodes were then applied following the procedure described earlier. For the cathode materials, two pieces of platinum mesh were co-sintered on both electrode surfaces to act as current collectors. Lead wires of Pt were used to connect the platinum-mesh current collectors to the measuring instrument. For the anode materials, pieces of nickel mesh were pressed over the electrode surfaces and co-sintered in a reducing atmosphere. Nickel lead wires were used to connect the nickel-mesh current collectors to the measuring instrument.

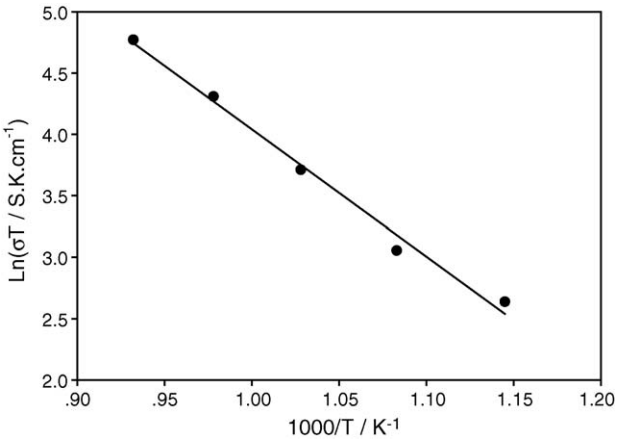

Fig. 2. Temperature dependence of the conductivity of LSGM electrolyte measured using the four-probe technique.

2.4. AC impedance characterization

The symmetrical cell was exposed to the same oxidizing (cathodic), or reducing (anodic) atmosphere on both sides and a two-probe configuration was used to measure the impedance spectra. During measurement a constant flow rate of air was maintained for experiments involving the cathode materials, and a constant flow rate of forming gas (95% argon–5% hydrogen) bubbled through water at 25 °C was maintained for experiments involving the anode materials. The measurements were made by applying a small-amplitude AC voltage (10 mV) to the cell and monitoring the response current as a function of the AC frequency (from 1 mHz to 65 kHz). A plot of the imaginary part of the measured impedance versus the real part reveals details of the individual ohmic and polarization contributions to the total

resistance of the cell. Impedance measurements were made in the temperature range of 600–800 °C in 50 °C increments for all the samples using a Perkin-Elmer potentiostat/galvanostat (model 263A) and Solartron analytical-frequency-response analyzer (model 1250).

The AC impedance measurements were performed on several cathode and anode materials including LSCF, LSCF–LSGM, LSM–LSGM, LSM, Ni–GDC, and Ni–LDC electrodes. For the Ni–GDC electrodes, measurements were made with and without the doped ceria (GDC/LDC) barrier layer. The Ni–LDC electrodes were evaluated with the LDC barrier layer. After the measurements, the samples were sectioned, epoxy mounted and polished. Optical microscopy and scanning electron microscopy were used to measure the grain size, porosity and thickness of the electrodes and confirm the consistency of the microstructure. Electron microprobe analysis and wavelength dispersive spectroscopy were also used to determine diffusion profiles of the elements at the interfaces.

2.5. Electrochemical characterization of complete SOFCs

Well-sintered dense LSGM electrolyte discs were ground to 1 mm thickness diamond paste. LDC paste was painted on one side of the LSGM electrolyte and sintered in air at 1300 °C for 4 h to act as the barrier layer between Ni–LDC anode and LSGM electrolyte. NiO–LDC (50% by volume of NiO) composite anode paste was then painted smoothly on the LDC barrier layer surface and sintered in air at 1300 °C for 2 h. After that, the LSCF–LSGM (50% by volume of LSCF) composite cathode paste was painted on the other side of the LSGM electrolyte and sintered at 1100 °C for 2 h. The effective electrode area of the cell was 1.33 cm^2, which was used for the current density calculation.

In order to decrease contact resistance at the anode, a Ni mesh was pressed over the anode surface and two separate nickel lead wires (current and voltage lead wires) were used to connect the nickel-mesh current collectors to the measuring instrument. Similarly, on the cathode side, a Pt mesh was sintered to the cathode at 900 °C by using a Pt paste (sintering time 1 h). Two separate lead wires of Pt (current and voltage lead wires) were used to connect the Pt-mesh current collectors to the measuring instrument. The test setup for the LSGM electrolyte supported SOFC is shown in Fig. 3. In this setup, gold O-ring was placed between the alumina tube and the LSGM electrolyte to seal the anode side. Thick Mica gasket was used on the cathode side as the seal. The assembled test cell was placed in the hot zone of a vertical furnace.

At the beginning of the tests, forming gas (95% Ar, 5% H_2) bubbled through water at room temperature was introduced on the anode side and an airflow was maintained on the cathode side. The temperature was then slowly increased to 800 °C. The NiO in the anode of the single cells was reduced by a stepwise replacement of the forming gas with hydrogen. The reduction was complete in 4 h in the hydrogen gas.

The electrochemical performance was measured between 600 and 800 °C in 50 °C intervals. The gas flow rate of hydrogen was 200 ml min^{-1} on the anode side and 150 ml min^{-1} of air on the cathode side. All electrochemical data were obtained by DC methods using a Perkin-Elmer potentiostat/galvanostat (model 263A). Electrochemical characterization consisted of measuring the open-circuit voltage (OCV) of the cells under SOFC operating conditions. The ratio of the measured OCV to the expected Nernst voltage provided a metric for determining the leak tightness of the cell. The current–voltage characteristics were measured with increasing current load from zero until the voltage dropped below 0.4–0.5 V. The electrical performance of these single cells were evaluated from the *I–V* plots by determining the ohmic loss, and the electrode polarization losses as a function of the cell current. Some experiments were conducted for longer times (5000 min) to determine performance stability. At the end of each test, microstructural characterization of the cells was performed. From these measurements, the overall stability and electrical performance of these cells were assessed.

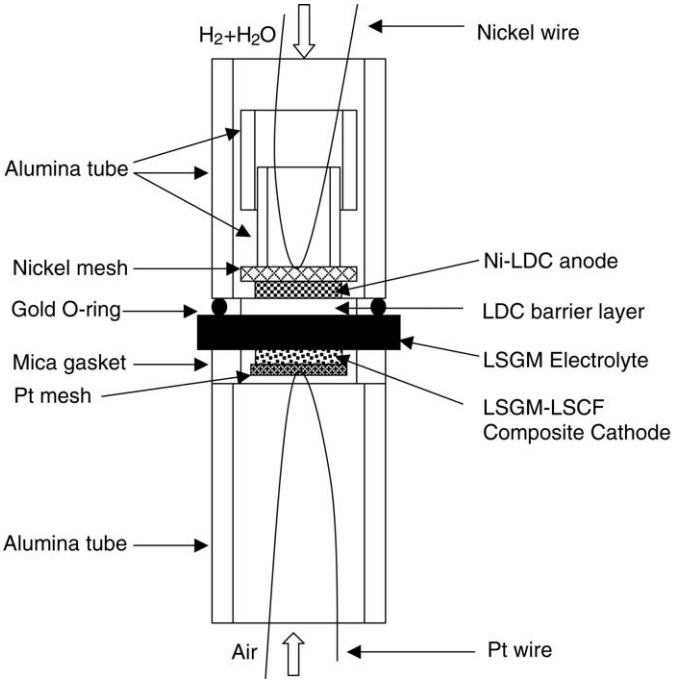

Fig. 3. Schematic of the setup employing LSGM-electrolyte-supported SOFCs for measuring electrical performance.

3. Results and discussions

3.1. Electrode microstructures

The microstructure of the composite cathode and anode is crucial to achieving high power densities while operating the cell. Fine microstructure, fine connected porosity and in the case of two-phase composite electrodes, well dispersed ionic and electronic conducting phases are essential for a satisfactory electrodes exhibiting low charge-transfer or interfacial polarization. It has been shown by Tanner et al. [21,22] that the effective charge-transfer resistance scales as the square root of the grain size of the electrode material. However, there is a limit to the acceptable pore size. When the electrode pore size is compa-

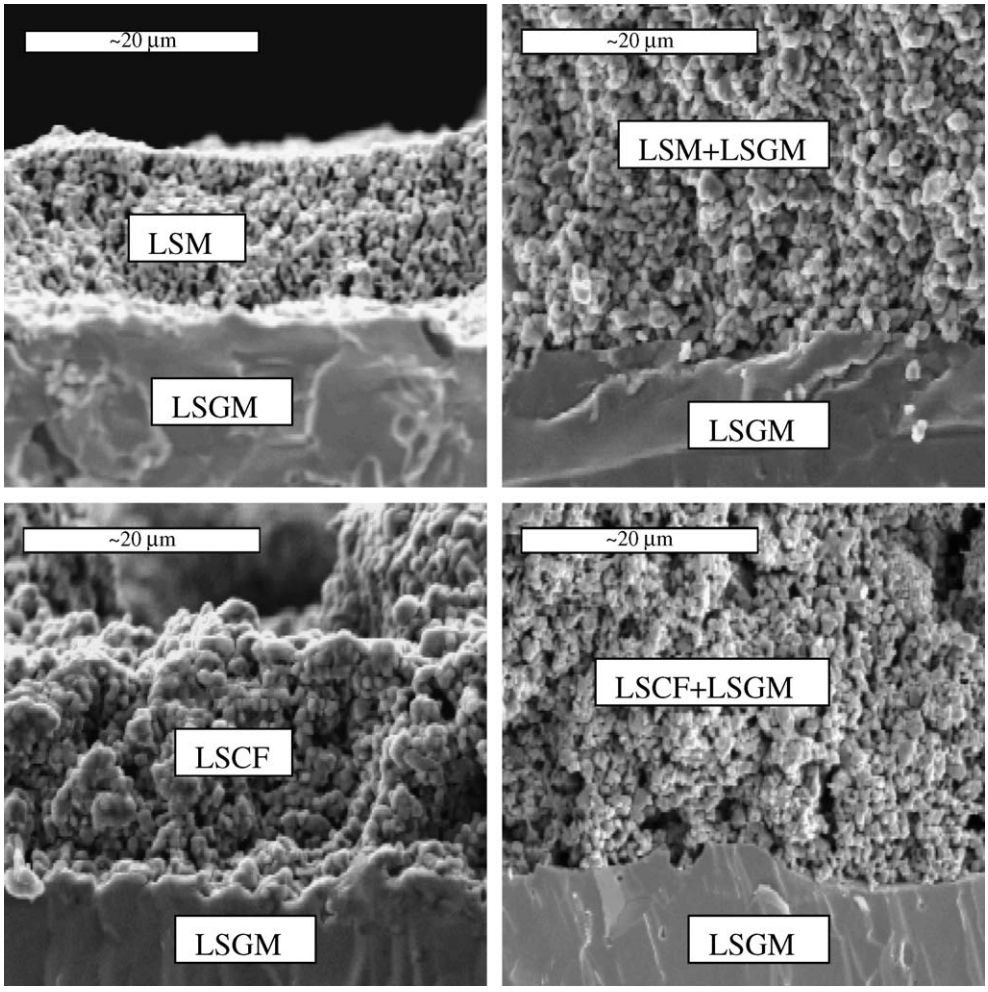

Fig. 4. SEM micrographs of fracture surfaces of cathode/electrolyte interfaces.

rable to the mean free path of the gases being transported in and out of the electrodes, gas diffusion through the pores will be mainly through the Knudsen diffusion mechanism and in this regime the cell performance is dominated by concentration (mass-transfer) polarization. To achieve a balance between these two conflicting requirements, graded electrode structures with a finer microstructure and porosity close to the electrolyte and coarser microstructure and larger porosity away from it needs to be developed for the supporting electrode. For instance, for an anode-supported SOFC, the fine electrode microstructure close to the electrolyte would have a large three-phase-boundary (ionic-electronic-gas) length and facilitate charge-transfer reactions and the coarser microstructure and porosity of the thicker outer anode layer would facilitate gas transport. This study is focused on the electrochemical characteristics of the layer with fine microstructure, that will be applied at the electrode interface with the electrolyte.

Fractured surfaces of the LSM, LSM–LSGM, LSCF, LSCF–LSGM, Ni–GDC, and Ni–LDC electrodes and their interfaces show that these electrodes have similar microstructures in terms of their interfacial adherence, porosity and grain size. The grain size is on the order of 1–2 μm and the porosity is between 25% and 35% which was measured optically from the micrographs using Adobe Photoshop software as well as the linear intercept technique. Sample cross sections of the fractured surfaces of various electrode/electrolyte interfaces are shown in Fig. 4. Based on the grain size, porosity and thickness (10–60 μm) of the electrodes, gas diffusion is not expected to control the interfacial polarization process particularly for small applied potentials that were used for the AC impedance measurements.

3.2. Impedance spectroscopy

A typical impedance plot measured using the symmetrical cell arrangement is shown in Fig. 5. For all samples measured in this investigation, a single depressed arc was observed. As discussed by previous workers [23–25], the high-frequency intercept of the impedance spectrum gives the ohmic resistance of the cell (R_{ohm}), which includes the resistive contributions of the electrolyte, the two electrodes, the current collectors and the lead wires. The low-frequency intercept gives the total resistance ($R_{ohm} + R_p$), which includes the ohmic resistance of the cell, concentration polarization (or mass-transfer polarization) resistance and the effective interfacial polarization resistance (R^{eff}_{redox}) associated with the electrochemical reactions at the

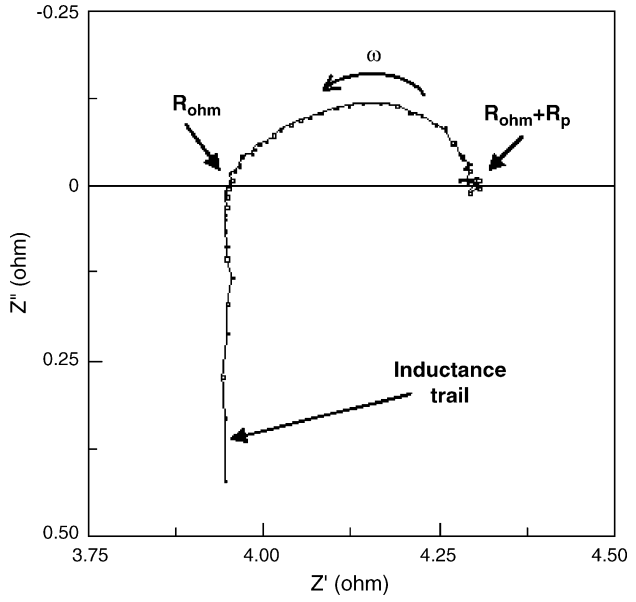

Fig. 5. A typical impedance plot of an LSGM symmetrical cell with identical electrodes (cathode/anode) at 800 °C.

electrode–electrolyte interface. The total polarization resistance of the electrode (R_p) is then extracted by subtracting the high-frequency intercept from the low-frequency intercept on the impedance plot. Given that the electrodes are thin, the amplitude of the applied AC voltage is small (10 mV), there was no DC bias present during the measurements, and the gas flow over the electrode was continuous, it is most likely that the effective interfacial polarization resistance, $R^{\text{eff}}_{\text{redox}}$, dominates the polarization resistance for the electrodes, i.e. the concentration polarization is negligibly small and R_p is essentially equal to $R^{\text{eff}}_{\text{redox}}$.

3.3. Selection of cathode material

In order to lower the interfacial polarization it is well known that the electrode needs to be a mixed conductor (have both electronic and oxygen ion conductivities) [4,13]. Since LSM is a p-type semi-conductor [4,26], it is advantageous to provide the oxygen-ion conductivity by mixing it with LSGM. On the other hand, since the LSCF is already a mixed conductor [27], mixing it with LSGM is not expected to significantly lower the interfacial polarization. However, it is to be noted that there is approximately 50% mismatch in thermal expansion coefficient between the LSCF electrode material ($19.5 \times 10^{-6}\,\text{K}^{-1}$) and LSGM electrolyte material ($11.6 \times 10^{-6}\,\text{K}^{-1}$) [11,12]. Therefore from the point of view of lowering the interfacial thermal stresses it is desirable to have a LSCF–LSGM composite electrode as the cathode. To explore these concepts, several cathode materials, LSM, LSCF, LSM–LSGM and LSCF–LSGM composite electrodes were studied for possible application in intermediate temperature (IT) SOFCs based on the LSGM electrolyte. Fig. 6 shows a comparison of the polarization resistances of the above cathode materials as a function of temperature measured using impedance spectroscopy on symmetric cells. The polarization resistance is plotted as inverse resistance versus

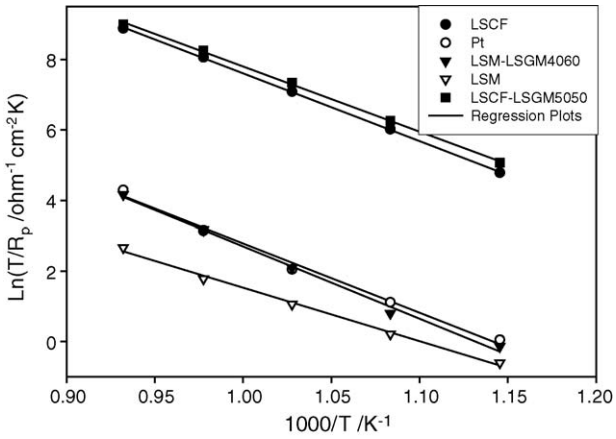

Fig. 6. Temperature dependence of the polarization resistance for various cathode materials measured in air.

inverse temperature. From these studies of cathode materials compatible with LSGM electrolyte it was determined that a 50 vol.% LSCF–LSGM porous composite would serve as the best cathode material. As can be seen from Fig. 6, the composite 50 vol.% LSCF–LSGM cathode has an interfacial polarization resistance that is several orders of magnitude lower than the LSM–LSGM composite cathode, although as expected the latter electrode has an interfacial polarization resistance that is lower than the conventional single-phase LSM electrode. The interfacial polarization resistance of the LSCF–LSGM composite cathode is also slightly lower than the single-phase LSCF cathode. In addition, considering the thermal expansion coefficient (TEC) mismatch between the LSCF cathode and LSGM electrolyte, the LSCF–LSGM composite is preferred over the single-phase LSCF material. Our investigations of mixed-conducting cathode materials have also revealed a dependence of polarization resistance on electrode thickness. The polarization resistance of LSCF cathode on LSGM electrolyte is shown as a function of thickness in Fig. 7. The polarization of the cathode layer initially decreases sharply with increasing electrode

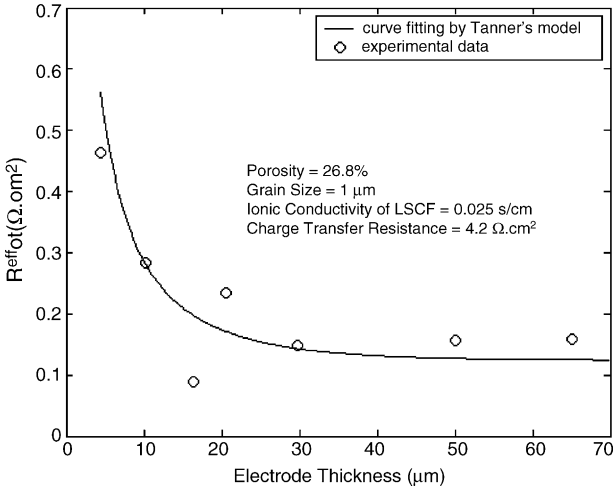

Fig. 7. A plot of interfacial polarization resistance as a function of electrode thickness for symmetrical LSCF/LSGM/LSCF cells measured in air at 800 °C.

thickness and then levels off asymptotically. The experimental results in Fig. 7 agree well with the model proposed by Tanner et al. [21,22]

$$R_p = R_{ct}^{eff} = \frac{L R_{ct}}{\left(\frac{1+\beta}{1+\beta e^{-2\frac{h}{\alpha}}}\right)(1-p)Le^{-\frac{h}{\alpha}} + \left(\frac{1+\beta e^{-\frac{h}{\alpha}}}{1+\beta e^{-2\frac{h}{\alpha}}}\right)\alpha\left(1-e^{-\frac{h}{\alpha}}\right) + pL} \quad (1)$$

where

$$\alpha = \sqrt{\sigma_{O^{2-}} L(1-p)R_{ct}} \quad \text{and} \quad \beta = \frac{\sigma_{O^{2-}} R_{ct} - \alpha}{\sigma_{O^{2-}} R_{ct} + \alpha} \quad (2)$$

in which $\sigma_{O^{2-}}$ is the ionic conductivity of the electrode; h the electrode thickness; p the porosity of the electrode; L the grain size of the electrode; R_{ct} is the intrinsic charge-transfer resistance given by

$$R_{ct} = \frac{RT}{ZFi_0} \quad (3)$$

where Z is the number of electrons participating in the electrode reaction, F the Faraday constant, R the gas constant, and T is the temperature. In fact, R_{ct} is a function of the electrochemical properties of the electrode/electrolyte pair, and also a function of the microstructure features of the electrode. Usually R_{ct} is treated as an empirical parameter, determined experimentally for a given electrocatalyst/electrolyte pair. It is evident from Fig. 7 that increasing the electrode thickness had the effect of decreasing the effective interfacial polarization resistance. Fig. 7 shows a fit to the data employing the model developed by Tanner et al. [22]. The fitting parameters are shown in Table 1.

The initial decrease of the cathode polarization resistance can be rationalized on the premise that increasing the electrode thickness results in an increase in the number of electrochemical reaction sites, i.e. total three-phase boundary length in the case of composite cathodes, or total connected pore surface area in the case of mixed ionic–electronic conductors. The subsequent leveling off of the polarization resistance is due to the fact that above a certain critical electrode thickness the migration of the oxygen ions from the reaction sites to the electrode/electrolyte interface become rate controlling. Thus, there is a certain critical thickness beyond which the cathodic polarization resistance shows no further decrease with increasing thickness. This critical electrode thickness has been shown to be a strong function of the microstructure (grain size) and porosity [21,22], i.e. finer the microstructure and finer the porosity, smaller the critical thickness. Based on our cathode microstructure, it is clear that a thickness of 40 μm is sufficient to minimize the interfacial polarization resistance.

Table 1
Curve fitting parameters for modeling electrode polarization as a function of electrode thickness

$\sigma_{O^{2-}}$ (S cm^{-1})	0.025
L (μm)	1
p (%)	26.8
R_{ct} (Ω cm^2)	4.2

3.4. Selection of anode material

Nickel is a well-known SOFC anode material, and acts as the fuel side electrocatalyst and current collector. GDC is an excellent oxygen-ion conductor, is chemically and mechanically compatible with the LSGM electrolyte and has electronic conductivity under reducing conditions [2,11,28]. Therefore, Ni–GDC cermet is expected to be an effective anode if its reaction with the LSGM electrolyte can be prevented. The reactivity of the Ni–GDC cermet anode with the LSGM electrolyte was studied by using the Ni–GDC/LSGM/Ni–GDC symmetrical cell at 800 °C under a reducing atmosphere (H_2-bubbled through 25 °C water bath). Both the ohmic and interfacial polarization resistances increased gradually with time, which is shown in Fig. 8. These results were used to confirm that this was due to Ni reacting with the LSGM and forming insulating phases (lanthanum nickelates) at elevated temperatures [14]. Therefore the use of a layer of doped ceria between the LSGM electrolyte and Ni–GDC anode to prevent direct contact between the Ni in the anode with the lanthanum in the LSGM electrolyte was investigated.

3.4.1. Ni–GDC electrodes with GDC barrier layer on LSGM electrolyte

It was apparent from the wavelength-dispersive-spectroscopy (WDS) analysis of these samples that the GDC barrier layer allowed lanthanum diffusion from the LSGM electrolytes (Fig. 9). Lanthanum diffusion from the LSGM electrolyte into GDC barrier layer leads to the formation of $Ce_{1-x-y}La_xGd_yO_2$ solid solution in the GDC barrier layer and resistive phases $LaSrLa_3O_7$ or $LaSrGaO_4$ at the LSGM electrolyte interface [29]. The latter significantly increases the ohmic resistance of the cell. By decreasing the sintering temperature of the GDC barrier layer it is possible to decrease the lanthanum diffusion, but this leads to incomplete densification and poor interfacial adherence of the GDC barrier layer to the LSGM electrolyte. This also causes

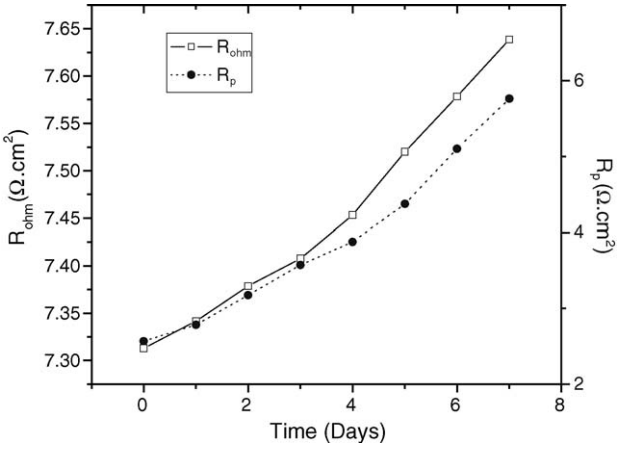

Fig. 8. Time dependence of ohmic and polarization resistances of symmetrical Ni–GDC/LSGM/Ni–GDC cell measured at 800 °C.

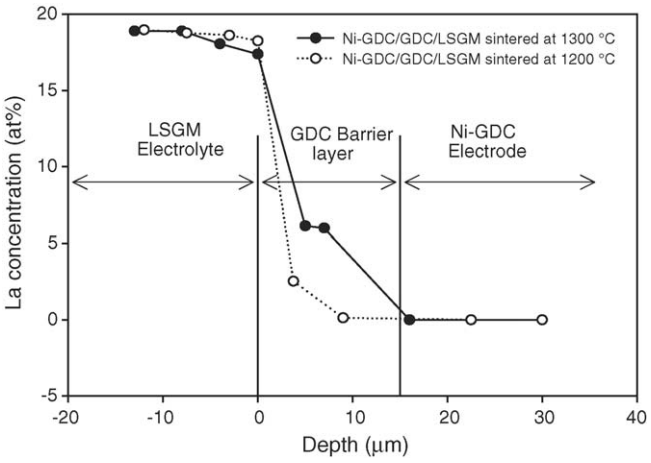

Fig. 9. Diffusion profile of lanthanum in the GDC barrier layer as a function of processing temperature.

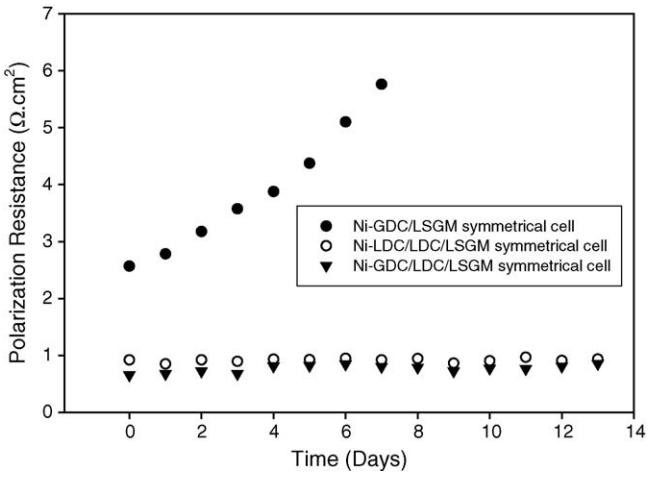

Fig. 10. Time dependence of the interfacial polarization resistances of cermet anodes with and without the LDC barrier layer over LSGM electrolyte at 800 °C.

penetration of the Ni–GDC anode slurry into the LSGM electrolyte surface through the porous GDC barrier layer and results in a time-dependent increase of the ohmic and interfacial polarization resistances similar to when the GDC barrier layer was absent. In conclusion, it was determined that the GDC layer did not serve as an effective barrier layer between the LSGM electrolyte and the Ni–GDC composite anode.

3.4.2. Ni–GDC and Ni–LDC electrodes with LDC barrier layer on LSGM electrolyte

Next, lanthanum doped ceria (LDC) was employed as the barrier layer between the LSGM electrolyte and the Ni-composite anode in order to limit or eliminate lanthanum diffusion from the LSGM electrolyte into the barrier layer. The idea was to eliminate or minimize the lanthanum chemical potential gradient at the interface that results in lanthanum diffusion. An important point of note is that unlike the LSGM electrolyte which has a perovskite phase, the LDC barrier layer has a fluorite structure. It is known from prior work that the Ni in the anode does not react with the lanthanum in the LDC barrier layer as long as the La content in the LDC is below 50 mol% in the cationic site [30]. It was observed that, unlike the GDC, when the LDC barrier layer had 40 mol% La in the Ce site and was sintered at 1300 °C, there was no detectable La diffusion from the LSGM electrolyte. The 40 mol% lanthanum doped ceria (LDC) likely has the same La chemical potential as in the LSGM and therefore prevented the La diffusion between LSGM electrolyte and the LDC barrier layer [30,31]. Also since the La content was below 50 mol%, it was expected to be stable in contact with the Ni-composite anode. Since LDC was being employed as the barrier layer, it was logical to also investigate Ni–LDC composite along with the Ni–GDC composite anodes. Time dependence of the interfacial polarization resistance at 800 °C of the LSGM symmetrical cells with Ni–LDC and Ni–GDC composite electrodes with LDC barrier layer is shown in Fig. 10. Also shown in the same figure is the interfacial polarization resistance of the Ni–GDC composite electrode without the barrier layer. The interfacial polarization resistances of both Ni–LDC and Ni–GDC electrodes with LDC barrier layer were stable over a period of 2 weeks, whereas the interfacial polarization resistance of the Ni–GDC electrode without the LDC barrier layer increased continuously with time due to the reaction between Ni and the lanthanum in the LSGM electrolyte. From the standpoint of chemical reactivity and thermal expansion coefficients it would thus be preferable to select Ni–LDC as the composite anode for the LSGM electrolyte with the LDC barrier layer.

3.5. Electrochemical performance of LSGM electrolyte supported cells

Based on the results of the electrode polarization studies, complete LSGM electrolyte supported SOFCs were fabricated for electrochemical evaluation. The cell components had the following dimensions and compositions:

(a) A 1 mm thick dense LSGM electrolyte.
(b) Dense adherent barrier layer (15 μm) of lanthanum doped ceria (LDC) between the LSGM electrolyte and the anode.
(c) A 50% by volume of Ni–LDC composite anode having a thickness of 30–40 μm and porosity of 25–35%.
(d) A 50% by volume of LSCF–LSGM composite cathode having a fine microstructure (1–2 μm grains), with a porosity of 25–35% and thickness of 30–40 μm.

The SEM micrographs of the polished cross section of a typical tested LSGM electrolyte supported SOFC are shown in Fig. 11. The tested cell had porous electrodes, dense electrolyte and well-bonded cell components. Although the LDC barrier layer was not always fully dense, the porosity appeared closed and it served its purpose.

The open-circuit voltages (OCV) at a given temperature in the tested cell were very close to the Nernst potential determined by the equation

$$\mathrm{OCV} = \frac{RT}{4F}\ln\left(\frac{P_{O_2(c)}}{P_{O_2(a)}}\right) \quad (4)$$

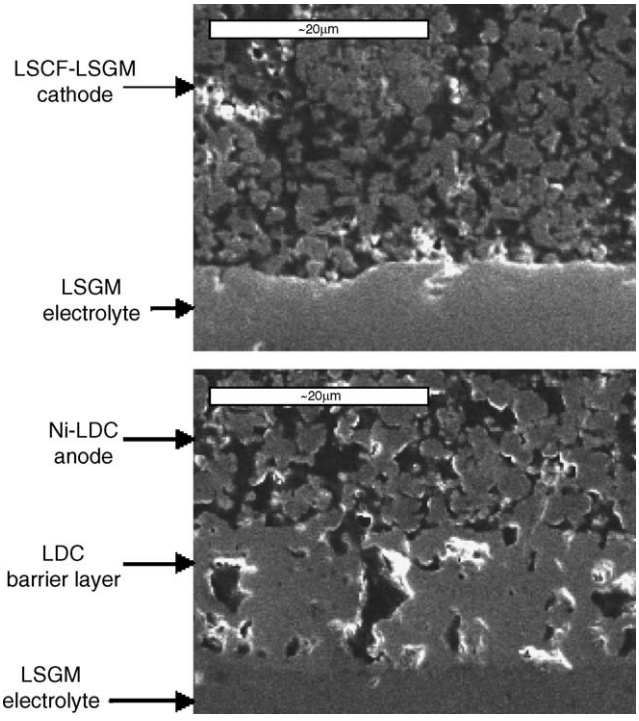

Fig. 11. SEM micrographs of the polished cross sections of the cathodic and anodic sides of the LSGM electrolyte supported SOFC that was electrochemically evaluated. LDC barrier layer was deposited on the anodic side.

where $P_{O_2(c)}$ is the oxygen partial pressure on the cathode side, and is 0.21 atm for air. $P_{O_2(a)}$ is the oxygen partial pressure on the anode side, and fixed by the H_2O to H_2 ratio at a given temperature. The calculated theoretical OCV for the cell at 800 °C is 1.116 V when hydrogen is bubbled through water at 25 °C (~3% water vapor). The measured OCV at 800 °C was 1.118 V, which was very close to the theoretical value. This result indicated good cell sealing. Shown in Fig. 12 is the dependence of the single cell voltages and power densities of the LSGM electrolyte-supported cell as a function of the current densities tested at 600, 650, 700, 750 and 800 °C. The maximum power

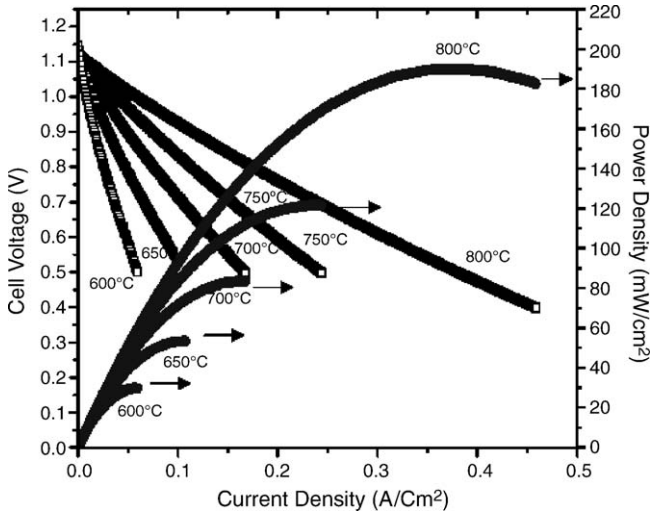

Fig. 12. Electrical performance of LSGM-electrolyte-supported (1 mm thick electrolyte) SOFC with a LDC barrier layer on the anodic side.

density ranged from 190 mW cm^{-2} at 800 °C to 30 mW cm^{-2} at 600 °C. The performance of the 1 mm thick present LSGM electrolyte supported cells are poorer than those in the work of Ishihara et al. who demonstrated approximately double the maximum power density at 800 °C [32,33] employing a thinner (0.5 mm thick) electrolyte. This demonstrates that it is possible to obtain improved power densities with thinner LSGM electrolytes.

3.6. Performance model for the LSGM electrolyte supported cells

Since the single cell testing were conducted with 1 mm thick electrolyte-supported SOFCs, the current and power densities were not very high (below 500 mA cm^{-2}). Both electrodes (cathode and anode) had high porosity and their thicknesses were small (around 30–50 μm), so the concentration polarization was negligible. The relationship between the cell voltage and current

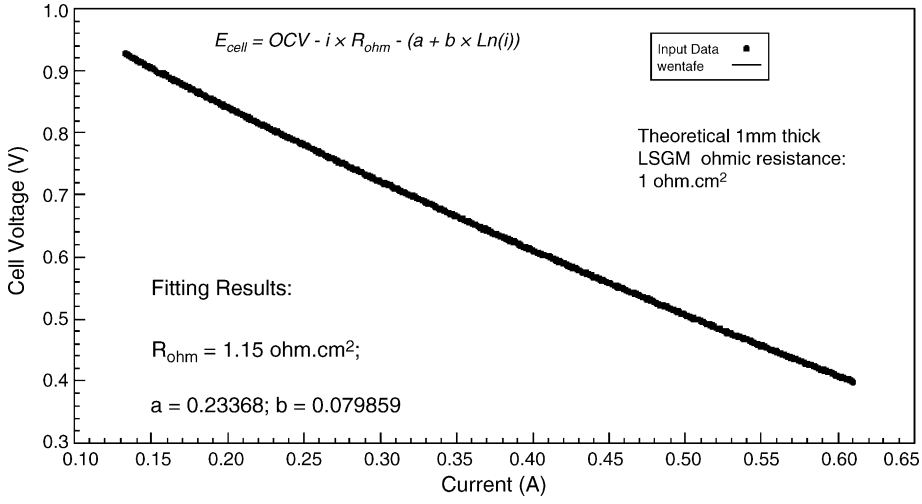

Fig. 13. Modeling electrode polarization from electrical performance data at 800 °C of LSGM-electrolyte-supported (1 mm thick electrolyte) SOFC with a LDC barrier layer on the anodic side.

Table 2
Curve fitting parameters for modeling electrode polarization

Temperature (°C)	R_{ohm} (Ω cm^2)	a	b	R_{el} (Ω cm^2)
800	1.148	0.23368	0.07986	1
750	1.8	0.2795	0.08777	1.43
700	2.45	0.3566	0.0988	2
650	3.972	0.3415	0.07666	3.353

density can be fitted as per the following equation [34]:

$$E_{cell} = OCV - iR_{ohm} - (a + b \ln i) \quad (5)$$

The experimental data was fitted to the above equation with three parameters, namely, R_{ohm}, a, and b. This assumes that apart from the ohmic losses (R_{ohm}) involving the electrolyte, electrodes, current collectors and the contact resistance, the only other loss associated with the electrodes are charge-transfer which is a function of the current as depicted by the Tafel term ($a + b \ln i$). Since the electrodes are relatively thin and the current density is small, losses due to concentration polarization at both cathode and anode have been assumed to be negligible. As seen in Fig. 13, Eq. (5) fitted the experimental data well at 800 °C. Similar fittings were obtained at other temperatures. Table 2 gives the parameters R_{ohm}, a, and b corresponding to the curve fitting results at other temperatures (from 650 to 800 °C). As mentioned earlier, R_{ohm}, consists of the ohmic resistances of the electrolyte, anode, cathode, current collectors, and the interfacial resistances between the electrodes and the electrolyte. The electrolyte resistance, R_{el}, can be calculated from its thickness (1 mm) and the ionic conductivity measured by the four-probe method (Fig. 2). It can be seen from Table 2, that R_{el} constitutes a substantial portion of R_{ohm}.

3.6.1. Performance stability

The performance stability of the LSGM electrolyte supported SOFC was evaluated by operating the cell at 800 °C starting with 0.72 V and a current density of 350 mA cm^{-2}. There was an initial 5% decay in the performance which is normally associated with the initial break-in period. The cell appears to stabilize after 3500 min (Fig. 14).

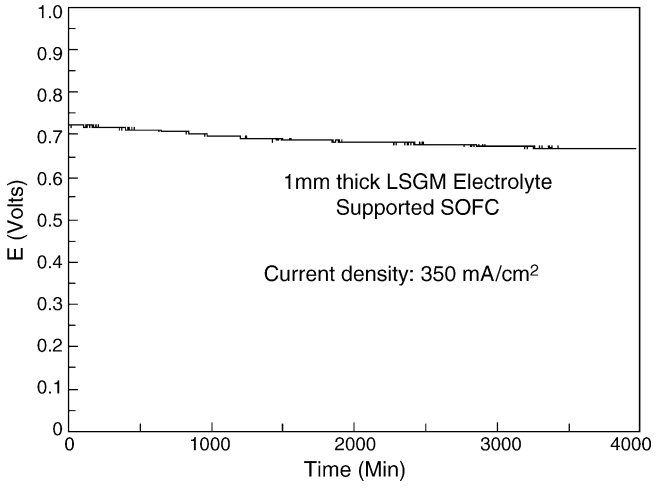

Fig. 14. Stability of the LSGM-electrolyte-supported SOFC with a LDC barrier layer on the anodic side (operating at 800 °C).

Higher power densities are expected with anode or cathode-supported thin film electrolyte SOFCs employing optimized electrodes, rather than the electrolyte supported SOFC as presented here. However, there are many challenges that need to be overcome to manufacture such electrode-supported cells based on the proposed materials system. The fact that the LSGM electrolyte sinters at a much higher temperature (1450 °C) compared to the anode (1200–1300 °C) and the cathode (1100 °C) would make the fabrication process difficult due to the increased reactivity between the components at 1450 °C. A variety of approaches to achieve these goals are presently being investigated and the results will be reported in a future publication.

4. Summary

The Sr- and Mg-doped lanthanum gallate (LSGM) offers the combination of highest ionic conductivity and materials stability under SOFC operating conditions. The cathode and anode materials for application in intermediate temperature (600–800 °C) SOFCs employing LSGM electrolyte had been studied. The cathode materials studied included, LSM, LSCF, porous composite electrodes comprising LSM–LSGM and LSCF–LSGM. It was found that the 50 vol.% porous composite of LSCF–LSGM was the best cathode material for the LSGM electrolyte. The investigation on mixed-conducting (ionic–electronic) cathode materials also revealed a dependence of polarization resistance on cathode thickness. The polarization of the cathode layer initially decreased sharply with increasing electrode thickness and then leveled off asymptotically beyond a critical thickness of 40 μm. This critical thickness is a function of the electrode microstructure. The fabricated cathodes typically had 1 μm average grain size and 30% porosity. Various anode materials were also studied. It was observed that Ni phase in the SOFC anode reacted with the perovskite LSGM phase to form an insulating lanthanum nickelate phase and this also caused the polarization resistance to increase with time. Therefore, the concept of applying a barrier layer to prevent direct contact and reaction of Ni with the LSGM electrolyte was investigated. GDC barrier layer allowed lanthanum diffusion from the LSGM electrolytes. However, LDC appeared to serve as an effective barrier layer between the LSGM electrolyte and the Ni-composite anode, because LDC had similar La chemical potential as in the LSGM, and the Ni in the anode did not react with lanthanum in the LDC barrier layer, which had a fluorite structure. Considering the chemical reactivity and thermal expansion coefficients, the Ni–LDC composite anode with a thin LDC barrier layer was the best anode material systems choice for the LSGM electrolyte.

Based on the cathode and anode materials studied, a 1 mm thick LSGM electrolyte supported SOFC was fabricated and electrically evaluated. It consisted of: Ni–GDC anode, LDC barrier layer between the anode and the electrolyte, LSGM electrolyte, and LSCF–LSGM composite cathode. The cell had a maximum power density of 190 mW cm^{-2} at 800 °C and 30 mW cm^{-2} at 600 °C. The electrochemical performance of the

cell was modeled and the model results were used to determine the nature of the polarization losses.

Acknowledgement

This paper was prepared with the support of the US Department of Energy, under Award No. DE-FG26-02NT41539. However, any opinions, findings, conclusion, or recommendations expressed herein are those of the authors and do not necessarily reflect the views of the DOE.

References

[1] S. Srinivasan, R. Mosdale, P. Stevens, C. Yang, Fuel cells, reaching the era of clean and efficient power generation in the twenty-first century, in: R.H. Socolow (Ed.), Annual Review of the Energy and the Environment, vol. 24, Annual Reviews, Pao Alto, CA, 1999, p. 281.
[2] N.Q. Minh, T. Takahashi, Science and Technology of Ceramic Fuel Cells, Elsevier Publishing Company Inc., New York, 1995.
[3] B.C.H. Steele, Solid State Ionics 75 (1995) 157.
[4] N.Q. Minh, Ceramic fuel cells, J. Am. Ceram. Soc. 76 (3) (1993) 563.
[5] S.C. Singhal, Recent progress in tubular solid oxide fuel cell technology, in: U. Stimming, S.C. Singhal, H. Tagawa, W. Lehnert (Eds.), Solid Oxide Fuel Cells V, The Electrochemical Society Proceeding Series, Pennington, NJ, 1997, p. 37.
[6] F. Zhao, A. Virkar, J. Power Sources 141 (2005) 79.
[7] Simens Westinghouse Brochure on SureCELL, Science and Technology Center, Pittsburgh, PA, 1996–2001.
[8] H. Kaneko, F. Jin, H. Taimatsu, J. Am. Ceram. Soc. 76 (1993) 793.
[9] K. Huang, R.S. Tichy, J.B. Goodenough, J. Am. Ceram. Soc. 81 (1998) 2565.
[10] S.P.S. Badwal, F.T. Ciacchi, D. Milosevic, Solid State Ionics 136/137 (2000) 91.
[11] J.-H. Kim, H.-I. Yoo, Solid State Ionics 140 (2001) 105.
[12] A. Petric, P. Huang, F. Tietz, Solid State Ionics 135 (2000) 719.
[13] M.T. Colomer, B.C.H. Steele, J.A. Kilner, Solid State Ionics 147 (2002) 41.
[14] X. Zhang, S. Ohara, R. Maric, H. Okawa, T. Fukui, H. Yoshida, T. Inagaki, K. Miura, Solid State Ionics 133 (2000) 153.
[15] M. Hattori, Y. Takeda, J.-H. Lee, S. Ohara, K. Mukai, T. Fukui, S. Takahashi, Y. Sakaki, A. Nakanishi, J. Power Sources 131 (2004) 247.
[16] W. Wang, A.V. Virkar, J. Power Sources 142 (2005) 1.
[17] J. Yoo, C.Y. Park, A.J. Jacobson, Solid State Ionics 175 (2004) 55.
[18] K. Huang, J.B. Goodenough, J. Alloys Compd. 303 (2000) 454.
[19] N. Trofimenko, H. Ullmann, Solid State Ionics 118 (1999) 215.
[20] J.W. Stevenson, T.R. Armstrong, L.R. Pederson, J. Li, C.A. Lewinsohn, S. Baskaran, Solid State Ionics 113 (1998) 571.
[21] C.W. Tanner, K.Z. Fung, A.V. Virkar, J. Electrochem. Soc. 144 (1997) 21.
[22] A.V. Virkar, J. Chen, C.W. Tanner, J.W. Kim, Solid State Ionics 131 (2000) 189.
[23] H. Hu, M. Liu, Solid State Ionics 109 (1998) 259.
[24] S. Wang, X. Lu, M. Liu, J. Solid State Electrochem. 6 (2002) 384.
[25] J.R. Macdonald, Impedance Spectroscopy: Emphasizing Solid Materials and Systems, Wiley, New York, 1987.
[26] N.Q. Minh, J. Am. Ceram. Soc. 76 (1993) 563.
[27] L.W. Tai, M.M. Nasrallah, H.U. Anderson, D.M. Sparlin, S.R. Sehlin, Solid State Ionics 76 (1995) 273.
[28] S. Sameshima, T. Ichikawa, M. Kawaminami, Y. Hirata, Mater. Chem. Phys. 61 (1999) 31.
[29] M. Hrovat, A. Ahmad-Khanlou, Z. Samardzija, J. Holc, Mater. Res. Bull. 34 (1999) 2027.
[30] K. Huang, J.H. Wan, J.B. Goodenough, J. Electrochem. Soc. 148 (2001) A788.
[31] Y. Matsuzaki, I. Yasuda, Solid State Ionics 152 (2002) 463.
[32] T. Ishihara, M. Honda, T. Shibayama, H. Minami, H. Nishiguchi, Y. Takita, J. Electrochem. Soc. 145 (1998) 3177.
[33] S. Wang, M. Ando, T. Ishihara, Y. Takita, Solid State Ionics 174 (2004) 49.
[34] A.J. Bard, L.R. Faulkner, Electrochemical Methods: Fundamentals and Applications, 2nd ed., John Wiley and Sons Inc., New York, 2001.